The microstructure and tensile properties of additively manufactured Ti-6Al-2Zr-1Mo-1V with a trimodal microstructure obtained by multiple annealing heat treatment

Sheng Zhang[a,b,*], Yuqi Zhang[a], Zhiyi Zou[c], Yusheng Shi[d], Yong Zang [a]

a School of Mechanical Engineering, University of Science and Technology Beijing, Beijing, 100089, PR China

b Shunde Graduate School, University of Science and Technology Beijing, Foshan, Guangdong, 528300, PR China

c Centre for Additive Manufacturing, University of Nottingham, Nottingham, NG8 1BB, UK

d State Key Laboratory of Materials Processing and Die & Mould Technology, School of Materials Science and Engineering, Huazhong University of Science and Technology, Wuhan 430074, China

*corresponding author. Tel: 86- 15201599409. E-mail address: zhangsheng@ustb.edu.cn

Abstract

Unlike acicular martensite, combining a lamellar and equiaxed α microstructure is known to impart high ductility for Ti-6.5Al-2Zr-1Mo-1V (TA15). In this article, we report innovative heat treatment aimed at optimizing the mechanical properties of additively manufactured TA15. After the proposed heat treatment, a trimodal microstructure consisting of equiaxed α, lamellar α, and a transformed β matrix was obtained. The resulting tensile properties were equivalent to those of forged TA15 counterparts. This paper discusses in detail the microstructure evolution involved in the heat treatment, as well as the microstructure–mechanical property relationships. The exceptional combination of strength and ductility obtained after the proposed heat treatment can allow the full exploitation of the additive manufacturing advantages of this excellent material.

Keywords： laser powder bed fusion; near-α Ti alloy; multiple heat treatment;

microstructure; mechanical properties

1. Introduction

Due to their high specific strength, excellent corrosion resistance, and superior weldability, titanium alloys are widely used in the aerospace, marine, and offshore oil and gas, automotive, medical, and chemical industries [1-3]. However, due to some inherent characteristics of titanium alloys, such as high chemical activity, high deformation resistance, poor workability, etc., the machining of titanium alloys is very difficult, which has become a major problem in the forming of titanium alloy parts. It is particularly prominent during the processing of complex structural parts [4]. The emergence of additive manufacturing technology can effectively solve this problem.

Laser powder bed fusion (L-PBF) is a new type of additive manufacturing technology. Recently, the laser powder bed fusion (L-PBF) additive manufacturing technique has proved to be a promising approach for manufacturing titanium alloys [5, 6]. L-PBF uses a focused high-energy laser to completely melt the metal powder and directly form metal parts through discrete + stacked lamination manufacturing, which greatly reduces production steps, reduces production cycles, and improves material utilization [7, 8]. In addition, due to its layer-by-layer stacking and manufacturing characteristics, it has the ability to produce net-shaped components with complex geometries in an affordable and eco-friendly way [9, 10, 11].

Over the past decade, a significant body of research has provided valuable insights into this manufacturing approach, with great emphasis placed on a particular titanium alloy–Ti-6Al-4V. This research has successfully demonstrated that, by optimizing process parameters, it is possible to print Ti-6Al-4V components with near-full density [12-14]. Due to the rapid cooling rate in the melted pool during the L-PBF process, the as-built microstructures of L-PBF titanium alloys are usually composed wholly or partly of metastable α’ [13, 15-18]. The high density of the lattice defects embedded in the metastable phase results in the high strength and low ductility of as-built L-PBF titanium alloys, limiting further application [18-21].

In response to this phenomenon, post-process heat treatments are often suggested as a powerful tool to tune the final microstructure and adjust the mechanical properties. Appropriate heat treatment can produce more favorable lamellar or equiaxed α/β features, improving ductility to a certain extent and allowing an acceptable strength–ductility combination to be obtained. As pioneers in related research, Vrancken et al. [6] examined traditional manufacturing processes and proposed heat treatment below the β phase transus temperature, which resulted in a relatively coarse α+β lamellar microstructure within the original prior-β grains, leading to significantly improved ductility. Recent research has demonstrated that, compared to conventional heat treatment, heat treatment tailored for additively manufactured material has the ability to further enhance the properties of L-PBF Ti-6Al-4V. Zou et al. [22] refined prior-β grains in L-PBF Ti-6Al-4V by rapid heat treatment. A significant increase in elongation at the break point (16.6 ± 0.7 %) was observed, with satisfactory yield stress (YS) and ultimate tensile strength (UTS). Sabban et al. [23] spheroidized the α grains using an innovative cyclic heat treatment strategy and obtained a bimodal microstructure, which enhanced ductility and toughness while maintaining the original high strength of the as-built material. Fan et al. [24] enhanced the tensile properties of L-PBF Ti-6Al-4V alloy using solution and aging heat treatment to finally obtain an improved combination of strength and ductility.

Compared to Ti-6Al-4V alloy, Ti-6.5Al-2Zr-1Mo-1V (TA15) alloy is an aluminum-equivalent alloy that approximates α titanium alloy, combining the merits of both α titanium alloy and α+β titanium alloy, such as good thermal strength and weldability, and excellent processing ductility [25]. It has a higher working temperature, better fracture toughness, a higher fatigue limit, better corrosion resistance, and improved welding performance compared to Ti-6Al-4V; therefore, it is widely used in the aerospace industry to manufacture load-bearing parts with complex structures that are expected to work in medium to high temperature conditions (up to 500 °C), whereas Ti-6Al-4V has a significantly reduced lifetime in such working environments [26]. It is widely accepted that using L-PBF to manufacture TA15 products can help to optimize the complex structure and improve the buy-to-fly ratio [27, 28], but due to

this being an emerging research topic, related understanding is still limited. Jiang et al. [4] obtained almost fully dense (99.98 %) L-PBF TA15 testing samples, and their strength–ductility combination was improved by heat treatment (800 °C/2 h/WC). Nevertheless, the ductility was still worse than for forged counterparts. Wu et al. [15, 18] obtained a better combination of UTS and elongation with optimized process parameters and heat treatment (750 °C/2 h/FC) of L-PBF TA15. Their research also suggested that the microstructure evolution of TA15 under the conducted heat treatment resembled that of Ti-6Al-4V. Wu et al. [29] further reported that both the width of the primary α and the volume fraction of the β phase increased with increasing soaking temperature, leading to improved ductility; however, a tradeoff between ductility and strength was also observed.

At the time of writing, the current research on the post-process heat treatment of as-built L-PBF TA15 still focuses on conventional single heat treatment. Although such heat treatment can improve the ductility of as-built TA15, the tensile properties still fail to meet the ideal standard (equivalent to forged counterparts); therefore, it can be assumed that more sophisticated heat treatment will be required to maximize the potential of as-built TA15. Following examination of the resulting tensile properties and microstructure, this paper proposes double and triple heat treatment as a means to achieve a superior combination of strength and ductility. It also discusses the microstructure evolution involved in the process, as well as the microstructure–mechanical property relationships of the as-built and heat-treated L-PBF TA15.

2. Materials and Methods

2.1. Materials used in this study

This study used vacuum-melted and gas-atomized TA15 powder provided by Beijing AMC Powder Metallurgy Technology Co., Ltd., China. The powder composition and particle size distribution are shown in Table 1 and Figure S1, exhibiting a nearly spherical morphology (Fig. S1a) and approximately normal distribution of the particle size (Fig. S1b). The average particle size of the powder was 43.6 μm (Fig. S1b).

Table 1

Chemical composition of the TA15 powder used in this study.

Element	Ti	Al	V	Zr	Mo	Si	Fe	Ni	Nb
wt.%	Balance	6.53	2.28	2.18	1.45	0.19	0.04	0.02	0.01

TA15 cylinders of Φ12 x 83 mm were printed vertically on the baseplate via EOS M280 using optimized parameters. An experimental approach determined the β transus temperature of the as-built TA15 material to be 995 ± 5 °C, as explained in detail in section 3.1.

2.2. Heat treatment of the as-built material

In this study, multiple heat treatments were applied to the as-built TA15 cylinders, as summarized in Table 2. Previous research has already suggested an optimized single heat treatment process for L-PBF TA15, involving soaking at a temperature of 750 °C to 800 °C for 2 h followed by air cooling (AC) [4, 15]; therefore, HT1 was conducted to establish a baseline for the comparison. For the proposed dual and triple heat treatment, 970 °C was selected as the soaking temperature for the primary annealing, since that temperature can effectively retain a high temperature β phase without excessive phase development [6, 30]. To achieve a good balance of the strength and ductility, the secondary annealing at 600-930 °C were applied to study the effect of the secondary annealing temperature on the mechanical properties. Finally, an aging treatment at 600 °C for 4 h was applied, which stabilized the microstructure and precipitates α precipitation to further improve performance. For all the conducted heat treatments, a heating rate of 10 °C/min was applied. For cooling, samples were taken out of the furnace and exposed to air. Single primary annealing (970 °C/1.5 h/AC) was also conducted to facilitate the study of the microstructure evolution during the heat treatments.

Table 2

The heat treatments conducted in this study.

No.	Primary annealing	Secondary annealing	Tertiary annealing
HT1	800 ℃/2 h/AC		
HT2	970 ℃/1.5 h/AC	600 ℃/3 h/AC	
HT3	970 ℃/1.5 h/AC	750 ℃/3 h/AC	
HT4	970 ℃/1.5 h/AC	850 ℃/3 h/AC	
HT5	970 ℃/1.5 h/AC	930 ℃/3 h/AC	
HT6	970 ℃/1.5 h/AC	930 ℃/3 h/AC	600 ℃/4 h/AC

2.3. Microstructure characterization and mechanical tests

The microstructural analyses in this study were conducted using an inverted optical microscope (OM, Zeiss Axio Imager 2), a scanning electron microscope (SEM, Zeiss GeminiSEM 500), and an electron-back-scattered diffraction technique (EBSD, JSM-7900F). Phase identification was carried out using an X-ray diffractometer (XRD, XRD-7000). The samples used for the microstructure characterization were polished with standard metallographic techniques. The OM and SEM samples were further etched using Kroll's reagent (HF, HNO_3; H_2O = 1:3:7) for 20 s to observe the microstructure. Samples for XRD were ground down to a finish by 5000-P SiC grinding paper. The working current and voltage were 35 KV and 40 mA respectively. The test parameters were: the diffraction angle range was 30 –90 °, and the scanning speed was 8 °/min. To improve the calibration rate, EBSD specimens were electrolytic-polished in a mixture of 8 % perchloric acid and 92 % ethanol solution at 20 ℃ and 27 V for 25 s. Image-Pro Plus 6.0 software was used for the quantification of the microstructures, including the volume fractions, aspect ratios, widths, and lengths of the phases.

Tensile testing was performed at room temperature on a tensile testing machine (MTS, CMT5205). Strain rates of 0.00025 s^{-1} (before yielding) and 0.0067 s^{-1} (after yielding) were applied up to the sample break point. The fracture morphology was then observed using SEM (Zeiss GeminiSEM 500). The as-built and heat-treated TA15 cylinders were machined into rod-shaped tensile specimens with a diameter of

Φ5 mm and a gauge length of 25 mm, according to the ISO 6892-1:2009 standard.

3. Results

3.1. β transus temperature of the L-PBF TA15 used in this study

According to JMatPro calculation, TA15 used in this study has a theoretical value of the phase transus temperature at approximately 994 ◦C. Using this temperature as a reference, the as-built TA15 samples were held at 980 ℃, 990 ℃, and 1,000 ℃ respectively, for 15 minutes, and then water-quenched. The resulting microstructures are shown in Figure S2. A strong resemblance was noticed, as shown in Figures S2a and b, with small amounts of primary α retained in the quenched microstructures. By contrast, only martensite α' was observed after quenching at 1,000 ℃ (Fig. S2c), indicating that the as-built material had been fully transformed to the β phase at 1,000 °C. Such observations suggested that the phase transus temperature of the material used in the study should be 990–1,000 ℃, corresponding to the theoretical value; therefore, the β transus temperature was determined as 995 ± 5 ℃.

3.2. Microstructures of L-PBF TA15 subjected to different heat treatments

3.2.1 Phase constituents of the as-built and heat-treated L-PBF TA15

The X-ray diffraction patterns of the as-built and heat-treated TA15 samples are presented in Figure 1. All the samples exhibited a typical α/α' martensite diffraction pattern, as indicated by the round dots. Both the α phase and α' martensite phase had hexagonal close-packed (HCP) lattice structures, which led to similar diffraction patterns. However, because the α' phase was obtained by rapid cooling from the β phase, the β stabilizer was unable to diffuse sufficiently during the cooling, resulting in a much higher amount of the β stabilization element retained in α' than in the equilibrium α phase. The supersaturated content caused a larger deformation of the α' crystal structure, resulting in broadening of its XRD diffraction peaks [4, 31]. The half-width of three main α/α' diffraction peaks under different conditions were calculated, as reported in Table 3. The half-widths of the α/α' diffraction peaks of the

untreated as-built TA15 sample were significantly higher than those of the heat-treated samples, suggesting that the corresponding diffraction peaks of the as-built sample were α' phase. Also, no β phase diffraction pattern was observed in the as-built sample, while the heat-treated samples all presented weak β (110) diffraction peaks, as indicated by the diamond dots. This indicated that, after heat treatment, the α' martensite phase in the as-built sample recovered to an equilibrium α+β phase.

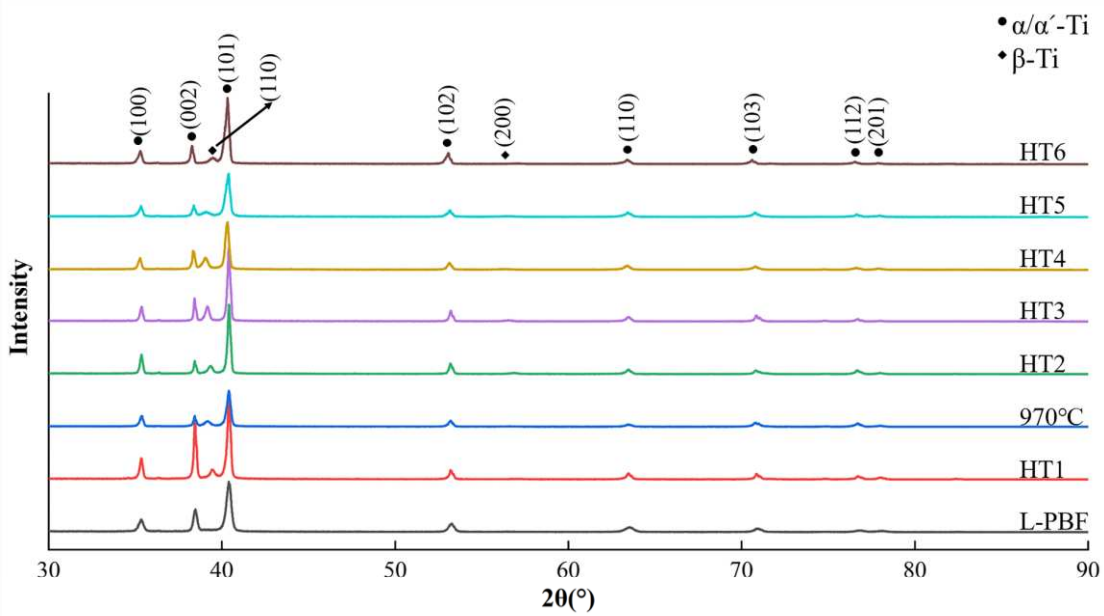

Figure 1. XRD spectra obtained from L-PBF TA15 subjected to different treatments. Round dots mark the reflections of the α phase, whereas diamond dots mark the reflections of the β phase.

Table 3

The half-widths of the three main α/α' diffraction peaks of L-PBF TA15 under different conditions.

Sample	Miller indices	(100)	(002)	(101)
As-built	2θ	35.33	38.47	40.39
	FWHM	0.356	0.279	0.358
HT1	2θ	35.34	38.45	40.40
	FWHM	0.231	0.200	0.249
970 ℃/1.5 h/AC	2θ	35.36	38.44	40.39
	FWHM	0.258	0.236	0.298
	2θ	35.35	38.44	40.41

HT2	FWHM	0.212	0.205	0.225
HT3	2θ	35.35	38.44	40.40
	FWHM	0.206	0.177	0.220
HT4	2θ	35.26	38.37	40.30
	FWHM	0.236	0.223	0.266
HT5	2θ	35.31	38.39	40.34
	FWHM	0.309	0.282	0.338
HT6	2θ	35.27	38.28	40.30
	FWHM	0.289	0.215	0.313

3.2.2 Morphological changes of the α structure as a function of heat treatment

Figure 2 presents microscopy images that demonstrate the typical microstructure of the as-built L-PBF TA15. No visible defects or pores were observed in the micrographs. Numerous columnar prior-β grains, parallel to the building direction, were observed in the XOZ plane, with widths of about 100–150 μm. The observed columnar grains were attributed to the fact that when the laser scanned the top layer of powder, its heat vertically penetrated several previously deposited layers, forming a temperature gradient parallel to the building direction and resulting in the directional growth of the prior-β grains [32]. Additionally, large numbers of acicular martensite α' phases with variable lengths were observed in the columnar prior-β grains due to the rapid cooling rate inside the melted pool during the printing process [18]. On the XOZ plane, these acicular structures were mainly distributed at an angle of ± 45° to the prior-β-grain boundaries, as shown in Figure 2b. This distribution corresponded to the (HCP lattice of the α' phase and related to a Burgers orientation relationship (BOR) between the α' and β phases [33].

It was also noticed that the martensite in the as-built microstructure had an obvious size difference [34], as shown in Figure 2b, which was believed to be the result of multiple thermal cycles in the L-PBF process [34]. Based on the length of the acicular needles, these martensites could be categorized as primary, secondary, tertiary, and

fourth α', as indicated in Figure 2b.

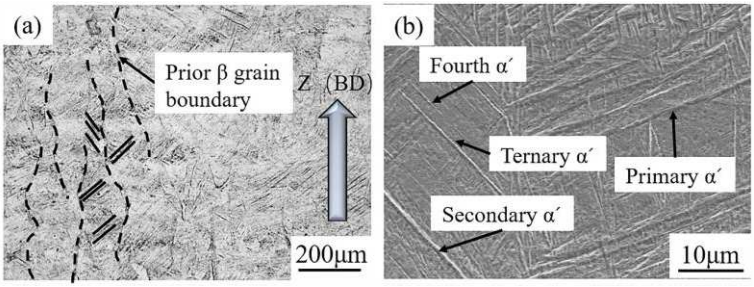

Figure 2. Typical microstructure of as-built TA15: (a) optical microscopy image of the XOZ plane, (b) SEM micrograph showing the size difference of the as-built martensite α'.

As a metastable phase, martensite α' contains dense crystallographic defects, such as deformation twins, annealing twins, and dislocations [34]. It is known that such a metastable phase, following equilibrium heating to a temperature above the martensite start temperature, will fully recover to a more stable α+β microstructure [34, 35], as shown in Figure 3a; therefore, after HT1, a basket-weave structure of lamellar α+β was observed in the microstructure.

During the laser melting process, due to the extremely rapid cooling rate, limited element diffusion occurred during the β to α' transformation, leading to the supersaturation of the β stabilizer (Mo, V) in α' [31, 35]. Such elements then gradually diffused during the equilibrium heat treatment, leading to the nucleation of the α phases at the martensite boundaries. Furthermore, development of the α phase formed a β stabilizer enriched area between the α lamellar phases, which then acted as the nucleation site of the β phase [36]. The observed basket-weave morphology after HT1 (Fig. 3a) was therefore related to the as-built α' arrangement shown in Figure 2b.

The microstructures obtained after other heat treatments are shown in Figures 3b–g. To provide a reference microstructure after the primary annealing, the as-built material was heat treated at 970 °C for 1.5 h and air cooled. Its microstructure, as presented in Figure 3b, consisted of short rod-shaped α grains (indicated by red arrows) and lamellar α+β grains. Of these, the short rod-shaped (or equiaxed) α grains were believed to be the primary α, while the lamellar α grains were assumed to be the

secondary α in the transformed β matrix. The average width of the short rod-shaped (or equiaxed) α was 3.84 ± 2.43 μm, with an aspect ratio of 6.47 ± 1.88.

Figures 3c–f show the microstructures obtained by HT2 to HT5, respectively, whereas Table 4 summarizes the grain sizes and aspect ratios of the short rod-shaped (or equiaxed) primary α under different conditions. After HT2 (Fig. 3c), a similarity was found between the final microstructure and the reference microstructure (Fig. 3b), with a noticeable coarsening of the primary α. The average width of the short rod-shaped (or equiaxed) α grains after HT2 was 4.28 ± 1.81 μm, like the reference status, whereas the aspect ratio decreased to 5.34 ± 3.32. As the secondary annealing temperature increased from 600 °C (HT2, Fig. 3c) to 930 °C (HT5, Fig. 3f), the primary α grains continued to coarsen. The average width of short rod-shaped (or equiaxed) α gradually increased from 4.28 ± 1.81 μm to 6.18 ± 2.62 μm, and the aspect ratio also decreased from 5.34 ± 3.32 to 2.71 ± 1.30. A notable globularization of the primary α grains occurred, with a more equiaxed morphology of the α structure appearing, as indicated by the red arrows in Figure 3f. Meanwhile, the secondary lamellar α in the transformed β matrix gradually became visually undetectable.

Figure 3g demonstrates the microstructure obtained after HT6 (the triple heat treatment). Compared with the double heat treatment of HT5 (Fig. 3f), the additional tertiary heat treatment did not significantly alter the microstructure. The average width of the obtained short rod-shaped (or equiaxed) α grains was 6.92 ± 2.02 μm, and the aspect ratio was 2.39 ± 1.17. The relatively low soaking temperature for the tertiary heat treatment (600 °C) made it act like a final aging process, which helped to fully diffuse the alloying elements, resulting in a more stable microstructure [37]. The achieved trimodal microstructure consisted of ~25 % equiaxed α, ~40 % lamellar (or short rod) α, and a transformed β matrix (as presented in detail in Fig. S3). According to research on traditional manufactured Ti alloys, the observed trimodal microstructure was highly likely to achieve a superior combination of high strength and high ductility [38-40].

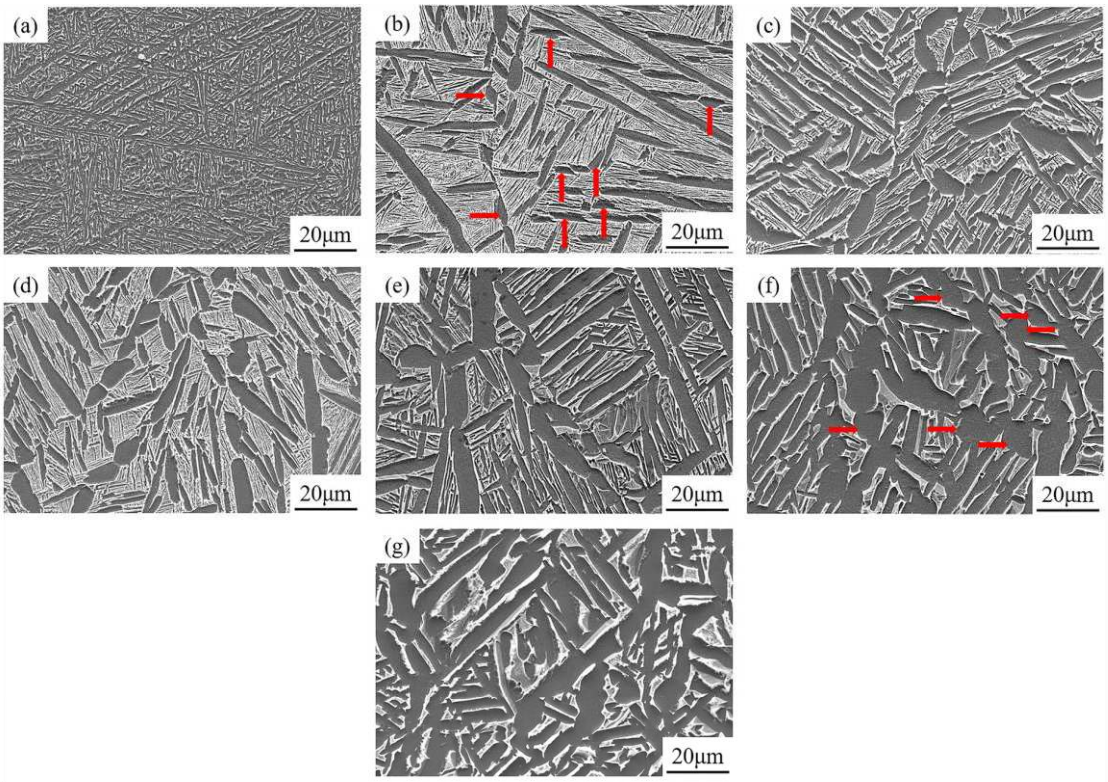

Figure 3. SEM images at a magnification of 1,000 showing the typical microstructures of L-PBF TA15 after various heat treatments: (a) HT1, (b) 970 ℃/1.5 h/AC, (c) HT2, (d) HT3, (e) HT4, (f) HT5, and (g) HT6.

Table 4

Grain sizes of short rod-shaped (or equiaxed) primary α and their corresponding aspect ratios after various heat treatments.

Heat treatment	Length (μm)	Width (μm)	Aspect ratio
970 ℃/1.5 h/AC	23.97 ± 13.865	3.84 ± 2.429	6.47 ± 1.878
HT2	22.85 ± 16.262	4.28 ± 1.814	5.34 ± 3.321
HT3	18.99 ± 12.099	4.54 ± 2.968	4.19 ± 2.144
HT4	16.69 ± 6.003	4.86 ± 1.730	3.66 ± 1.205
HT5	16.72 ± 6.544	6.18 ± 2.617	2.71 ± 1.304
HT6	16.55 ± 6.377	6.92 ± 2.024	2.39 ± 1.173

3.2.3 Crystallographic texture of L-PBF TA15 subjected to different heat treatments

Figure 4 presents the EBSD orientation maps and pole figures (PFs) on the XOZ plane under several typical conditions (as-built, HT1, HT5, and HT6). No visible changes were noticed on the prior-β structure; similar columnar morphologies with average widths of approximately 100–150 μm were observed under different conditions, marked by the black dotted line (the plotted prior-β grain boundary). However, significant differences in the α morphologies and the α grain sizes were observed, as shown in Figures 6a, c, e, and g, corresponding to the findings of the microscopy images reported in section 3.2.2. Due to the rapid cooling rate and complex thermal history, the as-built TA15 had extremely fine α' grains with an average grain size of 1.887 ± 1.272 μm [41]. Under different conditions, the coarsening of the α structure could be further verified by differences in the average sizes of the α grains, as reported in Table 5. The largest average size was 3.773 ± 4.293 μm, achieved after HT6.

The α PF of the as-built sample, as shown in Figure 4e, exhibited a weak HCP texture (maximum texture index of 5.575). Due to the BOR and the potential variant selection during the solidification in L-PBF process, multiple α/α' variants (typically 5 to 7 types) were derived from a single prior-β grain [42], resulting in the observed weak HCP texture of the as-built sample. After the proposed heat treatments, the HCP texture was significantly enhanced, as shown in Figures 4d, f, and h, indicating that the applied heat treatments had a notable impact on the α texture. This resulted from the recrystallisation and development of the α phase with the dominant prior-β-grain orientation during the equilibrium heating. Under the three conditions, the triple annealed sample had the strongest α texture, with a maximum texture index of 16.092.

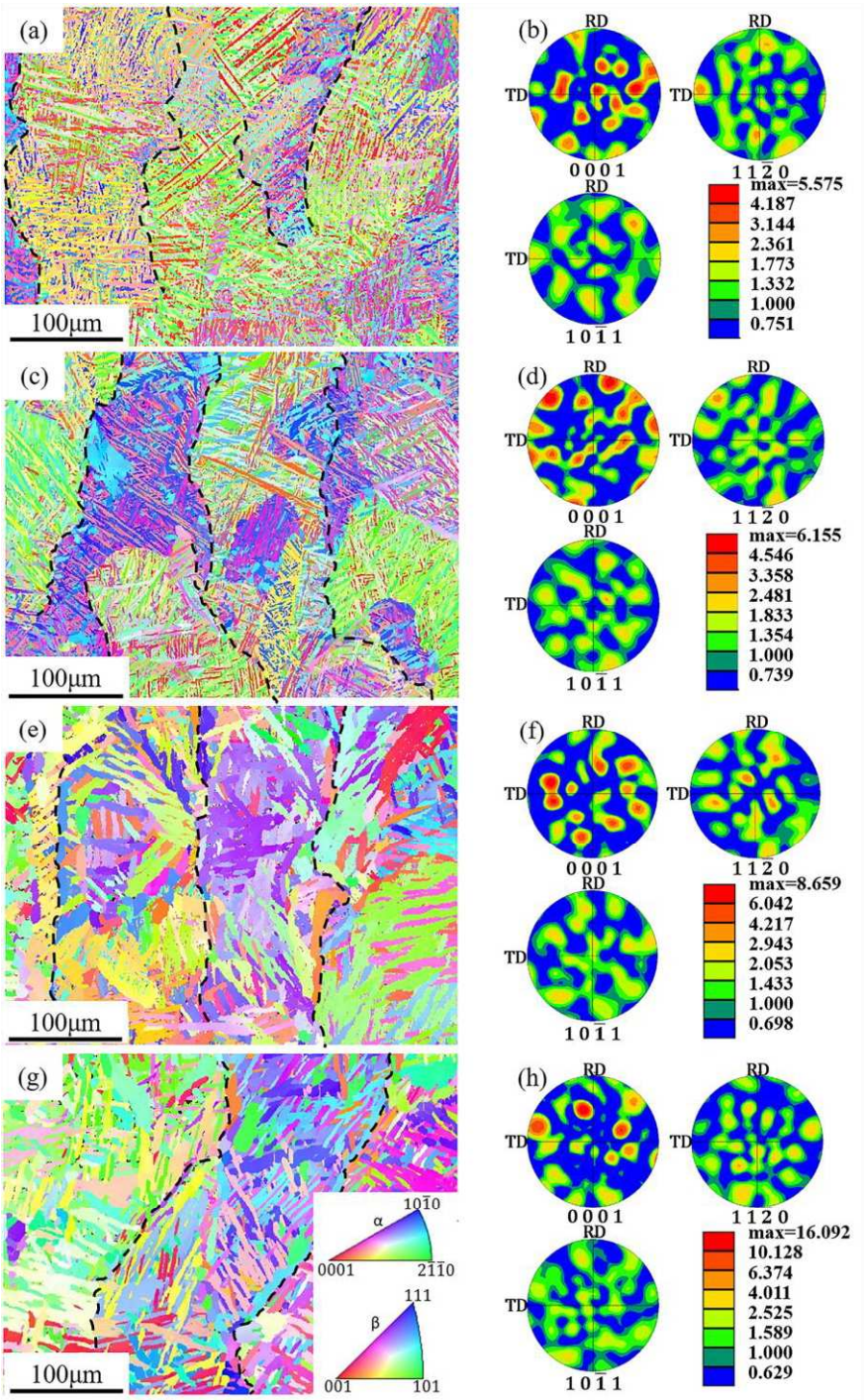

Figure 4. Typical α orientation maps at the XOZ surface and the corresponding PFs: (a, b) as-built TA15; (c, d) HT1; (e, f) HT5; and (g, h) HT6 samples.

Table 5

The average α/α’ grain sizes corresponding to the EBSD measurements shown in Figure 4.

	L-PBF	HT1	HT5	HT6
Average grain size (μm)	1.887 ± 1.272	1.889 ± 1.452	3.661 ± 2.475	4.293

3.3. Mechanical properties of L-PBF TA15 subjected to different heat treatments

3.3.1 Tensile properties

Significant differences between the α structures of L-PBF TA15 under different conditions suggested that the specimens may have behaved differently during the tensile testing. The stress-strain curves for all the conducted tensile tests are displayed in Figure 5, and the test results are reported and compared in Table 6.

The as-built specimen exhibited typical high strength (YS and UTS) and low ductility, whereas HT1 (single annealing) enhanced the ductility of the samples significantly, with elongations exceeding 14 %; however, a typical strength deficiency was observed. The dual heat treatments further improved the ductility, with a favorable secondary annealing temperature of 750 °C that enabled a ductility of ~16.68 % to be achieved; however, a similar decrease in strength was observed, which was associated with an increase in ductility. Of the conducted heat treatments, HT6 (the proposed triple heat treatment) provided the most favorable combination of strength and ductility, with an elongation of ~16.33 % obtained at the break point, a YS of ~934 Mpa, and a UTS of ~1,019 Mpa. Such tensile properties are equivalent to those of forged TA15 counterparts, which have a typical ductility of ~14 % to ~23 %, a YS of ~860 MPa to ~920 MPa, and a UTS of ~940 MPa to ~1,000 MPa [37, 38, 40, 43].

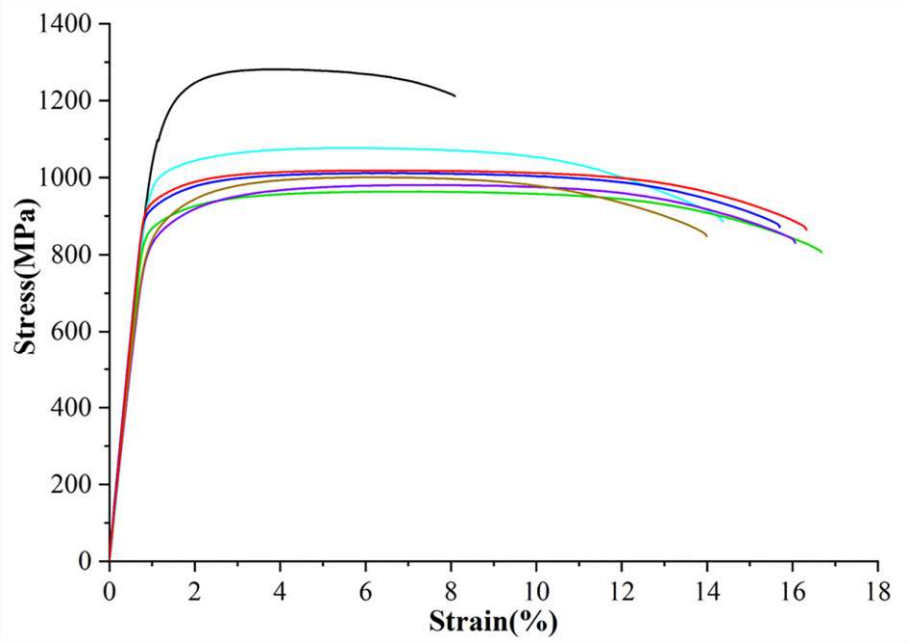

Figure 5. Stress-strain curves of L-PBF TA15 under different conditions.

Table 6

Measured mechanical properties of L-PBF TA15 under different conditions.

Samples	Ultimate tensile strength σ_u (MPa)	Yield strength σ_y (MPa)	Elongation ε (%)
L-PBF	1,281	1,123	8.14
HT1	1,077	993	14.37
HT2	1,012	917	15.70
HT3	964	868	16.68
HT4	981	834	16.06
HT5	1,001	838	13.99
HT6	1,019	934	16.33

3.3.2 Fracture morphology

To further understand the differences in the tensile behaviors of the L-PBF TA15, the tensile fracture behavior was analyzed, and the fracture morphology was observed, as shown in Figure 6 (further details have been provided in Figure S4). Figure 6a shows

the fracture morphology of the as-built TA15. The cleavage step, cleavage surface, and tear edge covered a significant portion of the fracture surface, whereas only a limited number of small dimples were found, suggesting that the material was brittle [44], consistent with the poor ductility (~8.14 %) of the as-built TA15. Figure 6b presents the fracture morphology of the TA15 sample after the single heat treatment (HT1). Compared with the as-built material, a significant increase in the dimples was noticed, accompanied by fewer brittle features, which reflected a typical ductile fracture, corresponding to the increase in ductility (~14.37 %) after HT1. Figures 6c and d show the fracture morphologies of the TA15 after the dual (HT5) and triple heat treatment (HT6), respectively. Similarities were observed across different fracture surfaces; increases in the sizes and depths of the dimples were observed, along with the appearance of many small dimples distributed around the large dimples, compared to the facture surface of the HT1 sample. This suggested more stable and reliable fracture behavior after dual and triple heat treatment [25].

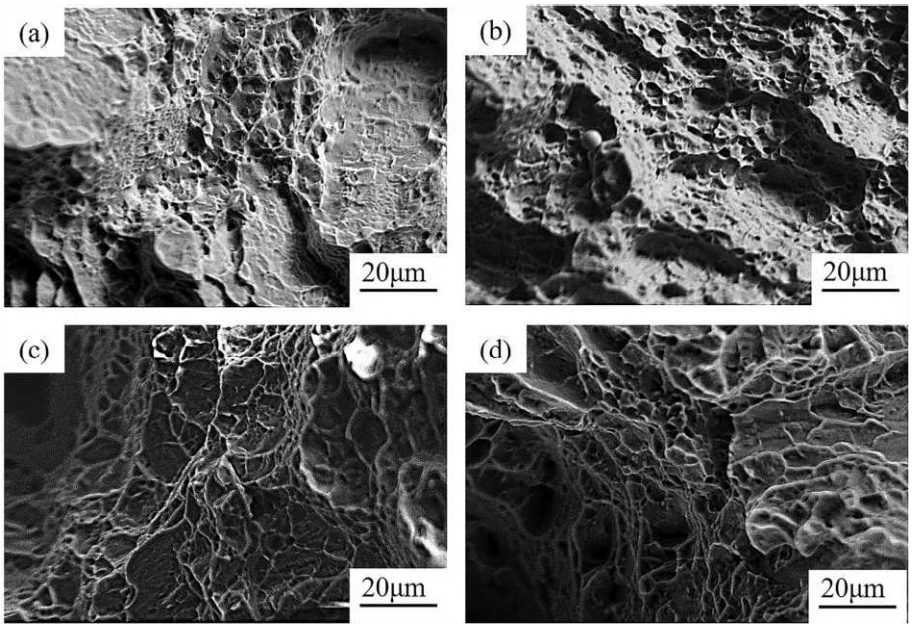

Figure 6. Fracture morphologies of L-PBF TA15 under different conditions: (a) as-built, (b) HT1, (c) HT5, and (d) HT6.

4. Discussion

4.1. Globularization of the primary α grains

The microstructure of the as-built L-PBF TA15 alloy mainly consisted of acicular martensite. After the proposed heat treatment, the as-built microstructure decomposed to an approximate trimodal microstructure, consisting of equiaxed α, lamellar α, and a transformed β matrix. During the process, coarsening, and globularization of the primary α grains were observed. A phenomenon normally reported in thermal-mechanical processed Ti alloys, this is considered to be a key factor leading to the superior mechanical properties of thermal-mechanical processed materials [38, 45]. This section discusses the possible mechanism resulting in the observed globularization.

Due to the rapid cooling rate during the laser melting process, the as-built martensitic α' contained very dense lattice defects, typically expressed by the large dislocation densities found after L-PBF in the core and at the boundary of the martensitic as-built microstructure [4, 18]. At an elevated temperature, these retained dislocations were activated, and their movement tended to reduce the Gibbs energy of the lattice system. This resulted in the formation of dislocation cells and walls within the α' or primary α grains. Ultimately, this progressed to the formation of the sub-grain boundary, as observed and reported in Zhao et al.'s research [30]. The supersaturated β stabilizer expelled from the α' or primary α concentrated at the newly formed subgrain boundary, leading to the development of the β phase at that location [22, 30]. Consequently, the original α'/α grain boundary could be weakened and possibly split. Also, the competitive growth of the primary α and the secondary α at high temperatures could further undermine the original α'/α grain boundary [45].

Due to the combined influence of the aforementioned factors, it could be assumed that holding L-PBF TA15 at an elevated temperature for a sufficiently long time would effectively split one original lamellar α into several α grains with much smaller aspect ratios. Furthermore, because the heating was uniform during the conducted heat treatment, the growth of such small α grains followed no preferred growth direction associated with the spatial coordinate system (XYZ). Such epitaxial growth of these α nuclei resulted in the observed equiaxed α in the microstructure after the proposed

heat treatment.

Since both the mobility of the dislocations and the growth rate of the α nuclei are hugely affected by temperature [30, 45], it could be deduced that altering the soaking temperature during the secondary annealing would effectively affect the volume fraction of the equiaxed α grains in the final microstructure. By comparing all the conducted dual heat treatments (HT2 to HT5), this study showed that a higher secondary annealing temperature led to a higher volume fraction of the equiaxed α grains. Finally, after soaking at 930 °C for 3 h during the secondary annealing, an approximate trimodal microstructure containing ~25 % equiaxed α, ~40 % lamellar α (short rod α), and ~35 % transformed β matrix was obtained. For the triple heat treatment (HT6), because the soaking temperature of the tertiary annealing was 600 °C—far below the β transus temperature—the final heat treatment only acted as an aging process, which did not significantly alter the resulting microstructure. The influence of such an aging process will be discussed in detail in section 4.2.

4.2. Microstructure–mechanical properties relationships

It is widely accepted that there is a direct link between the microstructures and mechanical properties of Ti alloys [46]; therefore, by tuning the achieved microstructure, heat treatment can effectively alter the final mechanical properties, as demonstrated by this study.

The as-built TA15 exhibited high-strength, low-plasticity performance, like other additively manufactured Ti alloys [23, 35, 47, 48]. The underlying mechanism for the observed tensile properties in the L-PBF TA15 alloy can be explained by the following strengthening mechanisms. The high density of lattice defects (dislocations, annealing twins, and deformation twins) is a typical feature of the acicular martensite structure. Since the material is already saturated with existing dislocations, newly developed dislocation will be prevented from nucleating. Such resistance to dislocation formation will be expressed as a resistance to plastic deformation during loading, resulting in the observed high strength [49]. As a type of crystal plane defect,

the nano-sized twin grain boundary can hinder the movement of dislocations and has the ability to accommodate dislocations [18]; therefore, the use of nano-sized twin grain boundaries can promote material strengthening [4, 15, 29]. Also, the thin lamellar β phase (nano-stripes) might be retained between the α’ laths (not found with XRD). The difference in the crystal structure and chemical composition of α’and β results in the concentration of stress at the α’/β boundary, further limiting plasticity [50]. Finally, refining grains has always been an effective way to strengthen polycrystalline materials [51]. As shown in Figures 2 and 4a, the microstructure of the L-PBF TA15 alloy L-PBF had extremely fine grains, with an average grain size of about 1.8 μm, which was much lower than that for forged and cast samples. Also, compared with equiaxed, lamellar, and short rod-shaped grains, α’ martensite had a large aspect ratio, which was slender and needle-like, and thus more conducive to increasing strength [52].

In this study, the prior-β structure was not altered by any of the conducted heat treatments. The latest in situ observation has suggested that, for heat treatments below the β transus temperature, the retained α laths pin the original prior-β grain boundaries, and therefore the overall β morphology remains unchanged [6]. Hence, it was reasonable to assume that the differences in the mechanical properties after various heat treatments would mainly be caused by differences in the achieved α structures.

After HT1, the ductility significantly improved, while the strength was only slightly reduced, corresponding to the fracture topography change shown in Figures 6a and b. This was associated with the coarser α+β lamellar structure transformed from the fine α′ acicular martensite. The β phase (BCC) had more slip systems than the α/α’ phase (HCP), resulting in improved plasticity after HT1 [4]. Additionally, the obvious reduction of crystal defects in the microstructure and the elimination of residual stress also resulted in decreased strength and improved plasticity. Finally, after HT1, the stress caused by the difference in composition between the β phase and the surrounding matrix α phase, and the dislocations accumulated at the grain boundary,

kept the material at a high strength.

After the proposed dual or triple heat treatment (HT2–HT6), a trimodal structure was obtained, which consisted of equiaxed α, lamellar α, and a transformed β matrix (with basket-weave secondary lamellar α inside). Studies have shown that equiaxed grains, lamellar grains, and the transformed β matrix in the trimodal microstructure contribute differently to the mechanical properties. The equiaxed grains play a coordinated role in deformation. When TA15 titanium alloy fractures, it has greater deformation and exhibits high plasticity, and its content is mainly affected by the heat treatment temperature [38, 53]. Lamellar grains are conducive to increasing the number of phase interfaces, leading to the improved strength and creep resistance of TA15 titanium alloy, and its content is determined by the temperature difference between the two heat-treatment steps [38]. The transformed basket-weave β matrix can cause the crack propagation of TA15 alloy to change in the direction of the lamellas and colonies during fracture, resulting in more crack branches and complex paths, increasing strength and toughness [23, 30, 40]. The combined effect of the three morphological structures affects the mechanical properties. The content of the three morphological structures can be adjusted by using different heat treatment parameters to control the strength and plasticity of the material. To obtain a better strength–plasticity combination, research on conventional manufactured Ti alloys has broadly recognized that a morphology close to, or even achieving, the perfect trimodal structure (consisting of ~15–20 % equiaxed α, 50–60 % lamellar α, and a transformed β matrix) tends to have better mechanical behavior than the lamellar structure [38, 40]. The lamellar structure obtained after HT1 was filled with lamellar α+β, and the lamellar grains were relatively slender. The trimodal structures obtained after HT2–6 contained equiaxed α, lamellar α, and transition β matrices, and the grains were obviously coarser. According to the Hall–Petch relation, a fine-grained microstructure facilitates superior strength [18]. Combining the influence of the mechanical properties of the three morphological structures mentioned above, the improvement of the plasticity of the trimodal structure could be attributed to the coarsening of grains, the appearance of equiaxed grains reaching a certain proportion, and the reduction of

lamellar grains. A certain number of lamellar grains and a transformed β matrix can ensure considerable strength, combining the merits of the basket-weave and bimodal microstructures and producing both high strength and high plasticity [38, 40].

Also, the latest research on the triple-heat-treatment additive manufacturing of titanium alloys has discovered the strengthening influence of a nano-scale submicroscopic structure on strength and plasticity [30]. During the stretching process, dislocation walls and channel structures formed in the primary α, and dislocation cells were observed in the secondary lamellar α. These dislocation walls and cell walls effectively hindered the movement of dislocations, resulting in high tensile strength. Moreover, the channel structures and the interiors of the dislocation cells provided a certain distance of glide for the mobile dislocation, which effectively blunted localized plasticity, thereby enhancing it. As stretching progressed, dislocation walls and dislocation cell walls were broken, and shear bands formed, which further enhanced plasticity. Moreover, a good shear band compensated for the strength reduction caused by dislocation walls and cell wall breakage. In summary, the appearance of the above phenomena in the stretching process further increased the strength and plasticity.

For the four types of conducted dual heat treatments (HT2–HT5), the microstructures remained lamellar structures after primary annealing at 970°C, and the primary α tended to transform into short rod shapes. Secondary annealing produced primary equiaxed α, forming a trimodal structure together with the original lamellar α and a transformed β matrix. Different soaking temperatures during the secondary annealing process resulted in different sizes and volume fractions of the primary α structures. The coarsening of the primary α was associated with a decrease in strength, which could be loosely explained by the Hall–Petch effect [51], whereas the increase in the short rod-shaped (or equiaxed) α volume fractions was associated with the observed increase in plasticity [37]. Moreover, the mechanical properties of the samples after double heat treatment clearly showed a trade-off between TA15 alloy strength and plasticity.

Finally, and notably, the triple heat treatment (HT6), with additional aging, successfully improved both the yield strength and ductility compared to HT5. Although such a difference cannot be attributed to any detectable difference in the microstructure, it is possible that the aging of Ti alloys can lead to the precipitation of nanometer-sized intermetallic particles. During the HT5 heat treatment process, the material underwent element segregation. The Al element was enriched at the α grain boundaries, resulting in decreased strength. Due to the high Al content, typical aging procedures (600 ℃/4 h/AC) resulted in the formation of nanometer-sized intermetallic particles through Ti_3Al precipitation (α_2), which increased the strength [54, 55]. Greater external stress was needed to make dislocation slip past the strengthening phase particles and continue to slip, hindering the dislocation slippage to a certain extent and providing additional precipitation strengthening. Simultaneously, aging can promote slip planarity, which is beneficial for improving plasticity [48, 54, 56]—a factor that is considered conducive to the mechanical behaviors of Ti alloys with trimodal structures.

5. Conclusion

The results presented in this article provide new insights into innovative heat treatments aimed at optimizing the mechanical properties of L-PBF TA15. After the proposed dual or triple heat treatment, trimodal microstructures consisting of equiaxed α, lamellar α, and transformed β matrices could be obtained. Such microstructures lead to tensile properties equivalent to those of forged TA15 counterparts, which conventional heat treatment of L-PBF has failed to achieve.

1. The interpretation of tensile data with a detailed microstructural investigation led to the following conclusions: The as-built L-PBF TA15 consisted of acicular martensite α’ and had high tensile strength and limited ductility.
2. Specimens to which a conventional heat treatment (HT1) was applied had lamellar α+β structures, leading to balanced tensile properties, with a typical trade-off between strength and ductility.

3. The proposed dual and triple heat treatment effectively resulted in trimodal microstructures, with improved strength and ductility. This was attributable to the formation of equiaxed primary α and a transformed basket-weave β matrix.

4. The globularization of the primary α was believed to be the result of the splitting of the original lamellar α and the following nondirectional phase development.

5. Aging benefitted the heat-treated specimens, suggesting the plausible influence of precipitation strengthening and element partitioning on the trimodal microstructures.

Credit authorship contribution statement

Sheng Zhang: Methodology, Resources, Writing - review & editing. **Yuqi Zhang**: Methodology, Writing - original draft, Investigation, Conceptualization, Characterization - review & editing. **Zhiyi Zou:** Methodology, Conceptualization, Writing - review & editing. **Yusheng Shi:** Resources, review & editing. **Yong Zang**: Resources, review & editing.

Declaration of competing interest

The authors declare that they have no known competing financial interests or personal relationships that could have appeared to influence the work reported in this paper.

Acknowledgements

This work was financially supported by the Fundamental Research Funds for the Central Universities (FRF-GF-20-10B) and Scientific and Technological Innovation Foundation of Foshan (BK20BE011).

Appendix A. Supplementary Material

Figures S1–S6 in the article are supplementary figures with related content and are

being submitted separately as supplementary materials, as follows:

Supplementary material.docx

References

[1] H. Attar, M. Calin, L.C. Zhang, S. Scudino, J. Eckert, Manufacture by selective laser melting and mechanical behavior of commercially pure titanium, Materials Science and Engineering: A. 593 (2014) 170-177. https://doi.org/10.1016/j.msea.2013.11.038.

[2] G.-C. Li, J. Li, X.-J. Tian, X. Cheng, B. He, H.-M. Wang, Microstructure and properties of a novel titanium alloy Ti-6Al-2V-1.5Mo-0.5Zr-0.3Si manufactured by laser additive manufacturing, Materials Science and Engineering: A. 684 (2017) 233-238. https://doi.org/10.1016/j.msea.2016.11.084.

[3] A.K. Syed, B. Ahmad, H. Guo, T. Machry, D. Eatock, J. Meyer, M.E. Fitzpatrick, X. Zhang, An experimental study of residual stress and direction-dependence of fatigue crack growth behaviour in as-built and stress-relieved selective-laser-melted Ti6Al4V, Materials Science and Engineering: A. 755 (2019) 246-257. https://doi.org/10.1016/j.msea.2019.04.023.

[4] J. Jiang, Z. Ren, Z. Ma, T. Zhang, P. Zhang, D.Z. Zhang, Z. Mao, Mechanical properties and microstructural evolution of TA15 Ti alloy processed by selective laser melting before and after annealing, Materials Science and Engineering: A. 772 (2020) 138742. https://doi.org/10.1016/j.msea.2019.138742.

[5] X.X. Wang, M. Zhan, P.F. Gao, H.R. Zhang, Micromechanical behaviour of TA15 alloy cylindrical parts processed by multi-pass flow forming, Materials Science and Engineering: A. 737 (2018) 328-335. https://doi.org/10.1016/j.msea.2018.09.062.

[6] B. Vrancken, L. Thijs, J.-P. Kruth, J. Van Humbeeck, Heat treatment of Ti6Al4V produced by Selective Laser Melting: Microstructure and mechanical properties, Journal of Alloys and Compounds. 541 (2012) 177-185. https://doi.org/10.1016/j.jallcom.2012.07.022.

[7] C. Cai, J.C.D. Qiu, T.W. Shian, C. Han, T. Liu, L.B. Kong, N. Srikanth, C.-N. Sun, K. Zhou, Laser powder bed fusion of Mo2C/Ti-6Al-4V composites with alternately laminated α'/β phases for enhanced mechanical properties, Additive Manufacturing. 46 (2021) 102134. https://doi.org/10.1016/j.addma.2021.102134.

[8] S. Sun, Q. Teng, Y. Xie, T. Liu, R. Ma, J. Bai, C. Cai, Q. Wei, Two-step heat treatment for laser powder bed fusion of a nickel-based superalloy with simultaneously enhanced tensile strength and ductility, Additive Manufacturing. 46 (2021) 102168. https://doi.org/10.1016/j.addma.2021.102168.

[9] C. Cai, S. Guo, B. Li, Y. Tian, J.C. Dong Qiu, C.-N. Sun, C. Yan, H.J. Qi, K. Zhou, 3D Printing and Chemical Dealloying of a Hierarchically Micro- and

Nanoporous Catalyst for Wastewater Purification, ACS Applied Materials & Interfaces. (2021) https://pubs.acs.org/doi/10.1021/acsami.1c14076.
[10] S.Y. Choy, C.-N. Sun, K.F. Leong, J. Wei, Compressive properties of Ti-6Al-4V lattice structures fabricated by selective laser melting: Design, orientation and density, Additive Manufacturing. 16 (2017) 213-224. https://doi.org/10.1016/j.addma.2017.06.012.
[11] L. Yang, S. Wu, C. Yan, P. Chen, L. Zhang, C. Han, C. Cai, S. Wen, Y. Zhou, Y. Shi, Fatigue properties of Ti-6Al-4V Gyroid graded lattice structures fabricated by laser powder bed fusion with lateral loading, Additive Manufacturing. 46 (2021) 102214. https://doi.org/10.1016/j.addma.2021.102214.
[12] G. Kasperovich, J. Hausmann, Improvement of fatigue resistance and ductility of TiAl6V4 processed by selective laser melting, Journal of Materials Processing Technology. 220 (2015) 202-214. https://doi.org/10.1016/j.jmatprotec.2015.01.025.
[13] L. Thijs, F. Verhaeghe, T. Craeghs, J.V. Humbeeck, J.-P. Kruth, A study of the microstructural evolution during selective laser melting of Ti–6Al–4V, Acta Materialia. 58(9) (2010) 3303-3312. https://doi.org/10.1016/j.actamat.2010.02.004.
[14] B. Zhou, J. Zhou, H. Li, F. Lin, A study of the microstructures and mechanical properties of Ti6Al4V fabricated by SLM under vacuum, Materials Science and Engineering: A. 724 (2018) 1-10. https://doi.org/10.1016/j.msea.2018.03.021.
[15] C. Cai, X. Wu, W. Liu, W. Zhu, H. Chen, J.C.D. Qiu, C.-N. Sun, J. Liu, Q. Wei, Y. Shi, Selective laser melting of near-α titanium alloy Ti-6Al-2Zr-1Mo-1V: Parameter optimization, heat treatment and mechanical performance, Journal of Materials Science & Technology. 57 (2020) 51-64. https://doi.org/10.1016/j.jmst.2020.05.004.
[16] J. Günther, S. Leuders, P. Koppa, T. Tröster, S. Henkel, H. Biermann, T. Niendorf, On the effect of internal channels and surface roughness on the high-cycle fatigue performance of Ti-6Al-4V processed by SLM, Materials & Design. 143 (2018) 1-11. https://doi.org/10.1016/j.matdes.2018.01.042.
[17] P. Kumar, O. Prakash, U. Ramamurty, Micro-and meso-structures and their influence on mechanical properties of selectively laser melted Ti-6Al-4V, Acta Materialia. 154 (2018) 246-260. https://doi.org/10.1016/j.actamat.2018.05.044.
[18] X. Wu, C. Cai, L. Yang, W. Liu, W. Li, M. Li, J. Liu, K. Zhou, Y. Shi, Enhanced mechanical properties of Ti-6Al-2Zr-1Mo-1V with ultrafine crystallites and nano-scale twins fabricated by selective laser melting, Materials Science and Engineering: A. 738 (2018) 10-14. https://doi.org/10.1016/j.msea.2018.09.087.
[19] W. Xu, M. Brandt, S. Sun, J. Elambasseril, Q. Liu, K. Latham, K. Xia, M. Qian, Additive manufacturing of strong and ductile Ti–6Al–4V by selective laser melting via in situ martensite decomposition, Acta Materialia. 85 (2015) 74-84. https://doi.org/10.1016/j.actamat.2014.11.028.
[20] X.-Y. Zhang, G. Fang, S. Leeflang, A.J. Böttger, A. A. Zadpoor, J. Zhou, Effect of subtransus heat treatment on the microstructure and mechanical properties of

additively manufactured Ti-6Al-4V alloy, Journal of Alloys and Compounds. 735 (2018) 1562-1575. https://doi.org/10.1016/j.jallcom.2017.11.263.
[21] H. Fan, S. Yang, Effects of direct aging on near-alpha Ti–6Al–2Sn–4Zr–2Mo (Ti-6242) titanium alloy fabricated by selective laser melting (SLM), Materials Science and Engineering: A. 788 (2020) 139533. https://doi.org/10.1016/j.msea.2020.139533.
[22] Z. Zou, M. Simonelli, J. Katrib, G. Dimitrakis, R. Hague, Refinement of the grain structure of additive manufactured titanium alloys via epitaxial recrystallization enabled by rapid heat treatment, Scripta Materialia. 180 (2020) 66-70. https://doi.org/10.1016/j.scriptamat.2020.01.027.
[23] R. Sabban, S. Bahl, K. Chatterjee, S. Suwas, Globularization using heat treatment in additively manufactured Ti-6Al-4V for high strength and toughness, Acta Materialia. 162 (2019) 239-254. https://doi.org/10.1016/j.actamat.2018.09.064.
[24] Z. Fan, H. Feng, Study on selective laser melting and heat treatment of Ti-6Al-4V alloy, Results in Physics. 10 (2018) 660-664. https://doi.org/10.1016/j.rinp.2018.07.008.
[25] Q.J. Sun, X. Xie, Microstructure and mechanical properties of TA15 alloy after thermo-mechanical processing, Materials Science and Engineering: A. 724 (2018) 493-501. https://doi.org/10.1016/j.msea.2018.03.109.
[26] S. Zhu, H. Yang, L.G. Guo, X.G. Fan, Effect of cooling rate on microstructure evolution during α/β heat treatment of TA15 titanium alloy, Materials Characterization. 70 (2012) 101-110. https://doi.org/10.1016/j.matchar.2012.05.009.
[27] W. Hintze, R. Schötz, J. Mehnen, L. Köttner, C. Möller, Helical milling of bore holes in Ti6Al4V parts produced by selective laser melting with simultaneous support structure removal, Procedia Manufacturing. 18 (2018) 89-96. https://doi.org/10.1016/j.promfg.2018.11.012.
[28] M. Simonelli, Y.Y. Tse, C. Tuck, Effect of the build orientation on the mechanical properties and fracture modes of SLM Ti–6Al–4V, Materials Science and Engineering: A. 616 (2014) 1-11. https://doi.org/10.1016/j.msea.2014.07.086.
[29] X. Wu, D. Zhang, Y. Guo, T. Zhang, Z. Liu, Microstructure and mechanical evolution behavior of LPBF (laser powder bed fusion)-fabricated TA15 alloy, Journal of Alloys and Compounds. 873 (2021) 159639. https://doi.org/10.1016/j.jallcom.2021.159639.
[30] Z. Zhao, J. Chen, H. Tan, G. Zhang, X. Lin, W. Huang, Achieving superior ductility for laser solid formed extra low interstitial Ti-6Al-4V titanium alloy through equiaxial alpha microstructure, Scripta Materialia. 146 (2018) 187-191. https://doi.org/10.1016/j.scriptamat.2017.11.021.
[31] E. Sallica-Leva, R. Caram, A.L. Jardini, J.B. Fogagnolo, Ductility improvement due to martensite α′ decomposition in porous Ti–6Al–4V parts produced by selective laser melting for orthopedic implants, Journal of the Mechanical Behavior of Biomedical Materials. 54 (2016) 149-158. https://doi.org/10.1016/j.jmbbm.2015.09.020.

[32] S.H. Mok, G. Bi, J. Folkes, I. Pashby, Deposition of Ti–6Al–4V using a high power diode laser and wire, Part I: Investigation on the process characteristics, Surface and Coatings Technology. 202(16) (2008) 3933-3939. https://doi.org/10.1016/j.surfcoat.2008.02.008.
[33] E. Aeby-Gautier, A. Settefrati, F. Bruneseaux, B. Appolaire, B. Denand, M. Dehmas, G. Geandier, P. Boulet, Isothermal α″ formation in β metastable titanium alloys, Journal of Alloys and Compounds. 577 (2013) S439-S443. https://doi.org/10.1016/j.jallcom.2012.02.046.
[34] J. Yang, H. Yu, J. Yin, M. Gao, Z. Wang, X. Zeng, Formation and control of martensite in Ti-6Al-4V alloy produced by selective laser melting, Materials & Design. 108 (2016) 308-318. https://doi.org/10.1016/j.matdes.2016.06.117.
[35] S. Cao, R. Chu, X. Zhou, K. Yang, Q. Jia, C.V.S. Lim, A. Huang, X. Wu, Role of martensite decomposition in tensile properties of selective laser melted Ti-6Al-4V, Journal of Alloys and Compounds. 744 (2018) 357-363. https://doi.org/10.1016/j.jallcom.2018.02.111.
[36] L. Zeng, T.R. Bieler, Effects of working, heat treatment, and aging on microstructural evolution and crystallographic texture of α, α′, α″ and β phases in Ti–6Al–4V wire, Materials Science and Engineering: A. 392(1) (2005) 403-414. https://doi.org/10.1016/j.msea.2004.09.072.
[37] Z. Sun, H. Wu, X. Ma, X. Mao, H. Yang, Dependence of Microstructure on Solution and Aging Treatment for Near-β Forged TA15 Ti-Alloy, Journal of Materials Engineering and Performance. 25(10) (2016) 4549-4560. https://doi.org/10.1007/s11665-016-2282-2.
[38] Z. Sun, H. Wu, Q. Sun, H. Yang, Tri-modal microstructure in high temperature toughening and low temperature strengthening treatments of near-β forged TA15 Ti-alloy, Materials Characterization. 121 (2016) 213-221. https://doi.org/10.1016/j.matchar.2016.10.010.
[39] Z.C. Sun, F.X. Han, H.L. Wu, H. Yang, Tri-modal microstructure evolution of TA15 Ti-alloy under conventional forging combined with given subsequent heat treatment, Journal of Materials Processing Technology. 229 (2016) 72-81. https://doi.org/10.1016/j.jmatprotec.2015.09.011.
[40] H. Wu, Z. Sun, J. Cao, Z. Yin, Formation and evolution of tri-modal microstructure during dual heat treatment for TA15 Ti-alloy, Journal of Alloys and Compounds. 786 (2019) 894-905. https://doi.org/10.1016/j.jallcom.2019.02.068.
[41] D. Ouyang, N. Li, W. Xing, J. Zhang, L. Liu, 3D printing of crack-free high strength Zr-based bulk metallic glass composite by selective laser melting, Intermetallics. 90 (2017) 128-134. https://doi.org/10.1016/j.intermet.2017.07.010.
[42] K. Wei, X. Zeng, G. Huang, J. Deng, M. Liu, Selective laser melting of Ti-5Al-2.5Sn alloy with isotropic tensile properties: The combined effect of densification state, microstructural morphology, and crystallographic orientation characteristics, Journal of Materials Processing Technology. 271 (2019) 368-376.

https://doi.org/10.1016/j.jmatprotec.2019.04.003.
[43] Z. Sun, Z. Yin, J. Cao, L. Huang, Allowable Ranges of Conventional Forging Parameters Determination for TA15 Ti-Alloy to Obtain Tri-modal Microstructure Under Given Subsequent Heat Treatment, JOM. 71 (2019) https://doi.org/10.1007/s11837-019-03837-6.
[44] Z. Liang, Z. Sun, W. Zhang, S. Wu, H. Chang, The effect of heat treatment on microstructure evolution and tensile properties of selective laser melted Ti6Al4V alloy, Journal of Alloys and Compounds. 782 (2019) 1041-1048. https://doi.org/10.1016/j.jallcom.2018.12.051.
[45] N. Stefansson, S.L. Semiatin, Mechanisms of globularization of Ti-6Al-4V during static heat treatment, Metallurgical and Materials Transactions A. 34(3) (2003) 691-698. https://doi.org/10.1007/s11661-003-0103-3.
[46] J. Li, H.M. Wang, Aging response of laser melting deposited Ti–6Al–2Zr–1Mo–1V alloy, Materials Science and Engineering: A. 560 (2013) 193-199. https://doi.org/10.1016/j.msea.2012.09.055.
[47] C. Qiu, N.J.E. Adkins, M.M. Attallah, Microstructure and tensile properties of selectively laser-melted and of HIPed laser-melted Ti–6Al–4V, Materials Science and Engineering: A. 578 (2013) 230-239. https://doi.org/10.1016/j.msea.2013.04.099.
[48] Z. Zou, M. Simonelli, J. Katrib, G. Dimitrakis, R. Hague, Microstructure and tensile properties of additive manufactured Ti-6Al-4V with refined prior-β grain structure obtained by rapid heat treatment, Materials Science and Engineering: A. 814 (2021) 141271. https://doi.org/10.1016/j.msea.2021.141271.
[49] Q.S. Pan, L. Lu, Strain-controlled cyclic stability and properties of Cu with highly oriented nanoscale twins, Acta Materialia. 81 (2014) 248-257. https://doi.org/10.1016/j.actamat.2014.08.011.
[50] A. Zafari, K. Xia, High Ductility in a fully martensitic microstructure: a paradox in a Ti alloy produced by selective laser melting, Materials Research Letters. 6(11) (2018) 627-633. https://doi.org/10.1080/21663831.2018.1525773.
[51] X. Wang, C. Wang, Y. Liu, C. Liu, Z. Wang, B. Guo, D. Shan, An energy based modeling for the acoustic softening effect on the Hall-Petch behavior of pure titanium in ultrasonic vibration assisted micro-tension, International Journal of Plasticity. 136 (2021) 102879. https://doi.org/10.1016/j.ijplas.2020.102879.
[52] P. Luo, D.T. McDonald, W. Xu, S. Palanisamy, M.S. Dargusch, K. Xia, A modified Hall–Petch relationship in ultrafine-grained titanium recycled from chips by equal channel angular pressing, Scripta Materialia. 66(10) (2012) 785-788. https://doi.org/10.1016/j.scriptamat.2012.02.008.
[53] Z. Sun, X. Li, H. Wu, H. Yang, Morphology evolution and growth mechanism of the secondary Widmanstatten α phase in the TA15 Ti-alloy, Materials Characterization. 118 (2016) 167-174. https://doi.org/10.1016/j.matchar.2016.05.020.
[54] C. Dichtl, Z. Zhang, H. Gardner, P. Bagot, A. Radecka, D. Dye, M. Thomas, R. Sandala, J.Q. da Fonseca, M. Preuss, Element segregation and α2 formation in

primary α of a near-α Ti-alloy, Materials Characterization. 164 (2020) 110327. https://doi.org/10.1016/j.matchar.2020.110327.
[55] L.R. Zeng, H.L. Chen, X. Li, L.M. Lei, G.P. Zhang, Influence of alloy element partitioning on strength of primary α phase in Ti-6Al-4V alloy, Journal of Materials Science & Technology. 34(5) (2018) 782-787. https://doi.org/10.1016/j.jmst.2017.07.016.
[56] S.S. Youssef, X. Zheng, Y. Ma, S. Huang, M. Qi, J. Qiu, R. Zhang, P. Hua, S. Zheng, J. Lei, R. Yang, Characterization of α2 Precipitates in Ti–6Al and Ti–8Al Binary Alloys: A Comparative Investigation, Acta Metallurgica Sinica (English Letters). 34(5) (2021) 710-718. https://doi.org/10.1007/s40195-020-01149-2.